Scientific Reports

https://doi.org/10.1038/s41598-026-38387-w

Article in Press

Effect of a truncated mutant factor V on hemostatic function and embryonic development in mice

Received: 9 September 2025

Accepted: 29 January 2026

Published online: 12 February 2026

Cite this article as: Miguel-Batuecas A., De Pablo-Moreno J.A., Porras N. *et al.* Effect of a truncated mutant factor V on hemostatic function and embryonic development in mice. *Sci Rep* (2026). https://doi.org/10.1038/s41598-026-38387-w

Andrea Miguel-Batuecas, Juan A. De Pablo-Moreno, Néstor Porras, Pablo Bermejo-Álvarez, Leopoldo González-Brusi, Luis J. Serrano, Javier M. De Pablo-Moreno, María José Sánchez, Mariano García-Arranz, Antonio Rodríguez-Bertos, Bilgimol Chumappumkal Joseph, Luis Revuelta & Antonio Liras

Effect of a truncated mutant factor V on hemostatic function and embryonic development in mice.

Andrea Miguel-Batuecas[§], Juan A. De Pablo-Moreno[§], Néstor Porras, Pablo Bermejo-Álvarez, Leopoldo González-Brusi, Luis J. Serrano, Javier M. De Pablo-Moreno, María José Sánchez, Mariano García-Arranz, Antonio Rodríguez-Bertos, Bilgimol Chumappumkal Joseph, Luis Revuelta[¥], Antonio Liras[¥].

Author information

Authors and Affiliations

Department of Genetics, Physiology and Microbiology, School of Biological Sciences, Complutense University, Madrid, Spain

Antonio Liras & Andrea Miguel-Batuecas

Department of Veterinary Sciences, School of Biomedical and Health Sciences, Universidad Europea of Madrid, Spain

Juan A. De Pablo-Moreno

VISAVET Health Surveillance Centre, Complutense University, Madrid, Spain

Néstor Porras, Javier M. De Pablo-Moreno & Antonio Rodríguez-Bertos

Animal Reproduction Department, "INIA, CSIC". Madrid, Spain

Pablo Bermejo-Álvarez & Leopoldo González-Brusi

Fundación Jiménez Díaz University Hospital Health Research Institute, Fundación Jiménez Díaz University Hospital, and Department of Surgery, Autonomous University, Madrid, Spain

Mariano García-Arranz & Luis J. Serrano

Centro Andaluz de Biología del Desarrollo (CABD), Consejo Superior de Investigaciones Científicas (CSIC), Junta de Andalucía (JA), Pablo de Olavide University (UPO), Sevilla, Spain

María José Sánchez

Department of Internal Medicine and Animal Surgery, School of Veterinary Medicine, Complutense University, Madrid, Spain

Antonio Rodríguez-Bertos

University of California San Diego, Department of Medicine, Division of Hematology/Oncology, La Jolla, California, USA

Bilgimol Chumappumkal Joseph

Department of Physiology, School of Veterinary Medicine, Complutense University, Madrid, Spain

Luis Revuelta & Juan A. De Pablo-Moreno

Corresponding author

Correspondence to Antonio Liras (aliras@ucm.es)

Contributions

[§]Authors have contributed equally as first authors. [¥]Authors have contributed equally to this work and share last authorship.

A.L. project administration and coordination, A.L., P.B.A., L.R. supervision, A.L., J.A.D.P.M., N.P., P.B.A., L.J.S. conceptualization, A.L., P.B.A., M.J.S., M.G.A., L.R. resources, A.L., P.B.A., M.G.A., A.R.B., L.R. funding acquisition, A.L., A.M.B., J.A.D.P.M., N.P., P.B.A., L.J.S., J.M.D.P.M., M.G.A., A.R.B. methodology, A.L., A.M.B., J.A.D.P.M., P.B.A., L.G.B., L.J.S., J.M.D.P.M., M.J.S., M.G.A., A.R.B., L.R, B.C.J. investigation, A.L., A.M.B., J.A.D.P.M., M.G.A, B.C.J. formal analysis and data curation and interpretation, A.L., A.M.B., J.A.D.P.M., N.P., P.B.A., L.G.B, B.C.J. writing – Original draft, A.L., A.M.B., J.A.D.P.M., N.P., P.B.A., M.G.A., L.R, B.C.J. writing – Review & Editing.

ABSTRACT

Factor V is an essential protein in the blood clotting process and plays a central role in secondary hemostasis. Its deficiency causes a rare inherited disorder characterized by episodes of severe bleeding, some of which can be life-threatening. Although previous studies have established that factor V is essential for normal embryonic development, its specific contribution to vascular maturation remains incompletely understood, factor V is believed to contribute to blood vessel stabilization and regulate angiogenesis through its interaction with thrombin. In a recent study, a CRISPR-engineered mouse model intended to produced a mild factor V deficiency disease, unexpectedly produced a frameshift mutation in the A3 domain, resulting in a truncated protein. Factor V levels in healthy embryonic mouse tissues were assessed to investigate its role at different developmental stages. The mutation markedly impaired viability, as homozygous mice exhibited a lethal phenotype with severe bleeding and perinatal death, along with impaired coagulation function. Histopathological and immunohistochemical analyses indicated a link between factor V deficiency, thrombin and α-smooth muscle actin, potentially affecting proangiogenic signaling and embryonic vascular formation. Factor V gene expression increased during late embryogenesis, underscoring its importance in vascular development and maturation. Overall, these findings are consistent with a role for factor V in stabilizing embryonic blood vessels and modulating thrombin-dependent angiogenesis, and add further detail on the developmental impact of its deficiency and the pathogenesis of congenital bleeding disorders.

Keywords Factor V, Factor V deficiency, Embryogenesis, Truncated mouse model, CRISPR/Cas9, Thrombin

Introduction

Hemostasis is a physiological process activated in response to endothelial damage with the main goal of forming a fibrin clot. The process comprises two stages: primary and secondary hemostasis, the latter being regulated by clotting factors, whose interaction

results in the formation of the fibrin clot [1,2]. Within secondary hemostasis, coagulation factor V (FV) plays a crucial role as both a procoagulant and an anticoagulant factor [3,4]. FV is a glycoprotein composed of 2224 amino acids organized into a single polypeptide chain (three A domains, one B domain and two C domains). It is produced and secreted mainly by hepatocytes and, to a lesser extent, by megakaryocytes [5-7], with average plasma concentrations of approximately 7 mg/dL in humans [7].

FV deficiency is an ultra-rare autosomal recessive disease associated with mutations in the *F5* gene. To date, over 200 mutations leading to the disease have been identified, missense mutations being the most common and the ones associated with less severe phenotypes. Notably, in exon 18 —where our variant is located— only missense and nonsense mutations have been reported [8,9]. In contrast, deletion mutations typically generate stop codons that result in more severe phenotypes [10,11]. FV deficiency is characterized by symptoms such as spontaneous mucosal and joint bleeds and, in severe cases, bleeding from internal organs.

The role of hemostasis during human embryonic development remains poorly understood. However, it is known that homeostasis is crucial to ensure vascular integrity during tissue formation. Remodeling of embryonic blood vessels includes differentiation of angioblasts, their alignment into solid vascular cords to form the primary vascular plexus and the subsequent generation of further endothelial cells which line central lumens [12]. Some authors have found differences between the hemostatic system of the fetus and that of newborns, noting that hemostatic mechanisms mature in a highly progressive manner [13-15]. The concentration of clotting factors in plasma varies across the different gestational phases, which supports the theory that the coagulation system matures during the embryonic and fetal phases [16-18].

Concentration of FV has been shown to increase by 45% in the human embryo [18], which has been directly associated with thrombin production [19]. Other authors have demonstrated that, apart from the liver, the spleen and the vascular endothelium, FV has also been identified in cytotrophoblasts and, to a lesser extent, in the chorionic villi [20].

In other species such as mouse (*Mus musculus*), FV exhibits about 80% homology with human FV, and the B domain being the least conserved part of the molecule given its removal upon activation of the protein [21]. FV plasma levels in mice are approximately 4.6 U/mL [22]; in coagulometric assays, mouse FV has been reported to show higher apparent activity than human FV [23]. Murine studies have demonstrated that FV is indispensable for embryogenesis and that insufficient levels of FV result in an impaired development of organs, blood vessels and the yolk sac, which leads to intra-abdominal bleeds and prenatal or neonatal death [24]. A FV-deficient model for the zebra fish showed high mortality rates among embryos and larvae [25]. However, even very low plasma levels of FV are able to prevent spontaneous bleeds and embryonic alterations [26]. By generating a missense mutation in a murine model —a recent study by our research group— succeeded in emulating a human mutation producing viable animals with no spontaneous bleeds, normal litter sizes, no deaths, and a mild phenotype of the disease as determined by coagulometry [27].

Thrombin is an essential molecule in the coagulation cascade and during embryogenesis, with a direct relationship with FV. The prothrombinase complex catalyzes the conversion of prothrombin into thrombin, activating PAR1 receptors, which are involved in the development of the yolk sac, vascularization and embryonic growth [28-31]. PAR1-deficient mouse embryos are prone to develop blood vessel abnormalities in the yolk sac as well as defects in the walls of large blood vessels,

which underscores the importance of these receptors during embryonic development [28,29].

The lethality associated with FV-deficient models has stood in the way of developing preclinical trials and therapies for this deficiency. For that reason, it is essential to further characterize the role of FV during embryogenesis to clarify how severe FV loss-of-function compromises vascular development and embryonic survival in mice.

The present study evaluated the effects of a frame-disrupting mutation occurring in the A3 domain of factor V in a mouse model. The mutation, which occurred in our laboratory as an off-target effect during application of the CRISPR/Cas9 system to generate a mild-phenotype FV-deficient mouse model [27], alters the reading frame of the *F5* gene.

Materials and methods

Animals

All animal experimentation was carried out in compliance with Spanish Royal Decree 53/2013 and EU Directive 2010/63/UE. The generation of the line and initial experimental protocols were approved by the Ethics Committee of the Veterinary School of the Complutense University of Madrid, the Ethics Committee for Animal Experimentation of the Complutense University, the Ethics Committees of the Spanish Institute for Agricultural and Food Research and Technology (INIA) and of the Madrid Regional Government (PROEX 358.4/21, PROEX 040/17). Embryogenesis experimentation was approved by the Ethics Committee, the authorizing body of the Pablo de Olavide University and the Ministry of Agriculture, Fisheries and Rural Development of Andalusia (approval code 03/05/2018/064). CBAxC57BL6 hybrid mice

were maintained on a 12-12-hour light/dark cycle at an optimal temperature of 19-20ºC with *ad libitum* access to food and water. All mice used in this study were bred in-house at the animal facilities of the participating institutions. At the end of the experiment, mice were sacrificed using CO_2 exposure, with death confirmed by cervical dislocation, and all efforts were made to minimize suffering. Experiment was carried out under strict veterinary control. This study is reported in accordance with the ARRIVE guidelines (Essential 10).

Generation of animal model

The FV frame-disrupting mutation (termed FVFD) was generated as a byproduct allele generated by non-homologous end joining when attempting a CRISPR-mediated insertion by homology directed repair to introduce a specific (Thr1857Met) following the methods as described [27].

Briefly, mouse zygotes were microinjected with Cas9 encoding mRNA, a sgRNA targeting FV and a donor ssDNA containing Thr1857Met mutation. Following microinjection, embryos were cultured to blastocyst stage and then transferred to pseudo pregnant recipients following the uterotubal technique as described [32].

Genotyping

The genomic DNA samples from ear biopsy (punching) of the surviving pups were processed following previously described protocols to prepare high-resolution sequencing libraries [27,33]. The primers used are listed in Table 1.

	Construct (5′→3′)	Access number	WT bp
Forward	[a]*TCGTCGGCAGCGTCAGATGTGTATAAGAGACAG* AGAGAGCTCCGTCACAACAT	NC_000067.7	358
Reverse	*GTCTCGTGGGCTCGGAGATGTGTATAAGAGACAG* GCCCGTCTTCACATTTTCACA	NC_000067.7	358

Table 1. Genotyping primers. [a]llumina MiSeq System sequencing overhangs are identified in italics within the genotyping primers; WT bp: size of the wild-type product expressed in base pairs.

A female founder with the target mutation (Thr1857Met), described and developed in the previously stated model designed by our laboratory [27], as well as an allele containing a 4 bp frame-disrupting indel that truncated the protein at the residue 1851 (termed FVFD allele), was mated with a WT male. This resulted in F1 heterozygous carriers (Hz) for FVFD mutation, which were intercrossed to obtain WT animals, heterozygous (Hz) and homozygous (Hm) individuals for FVFD. Subsequent genotyping was carried out by Sanger sequencing of purified PCR products.

Blood collection

An initial study was planned with 6 WT, 6 Hz and 6 Hm mice, for FVFD mutation in both sexes (1:1 male-female proportion), but only WT and Hz individuals could be analyzed due to Hm mice mortality. Blood extraction was performed manually, without anesthesia, during the first 6 hours of the light cycle. A 23G needle was used to puncture the submandibular venous sinus and 0.25 mL of blood was collected in tubes filled with sodium citrate 3.2% (0.109 M, Vacutest Kima, Padua, Italy). The samples were centrifuged at 2,500xg for 15 min at 20°C, and aliquoted for immediate analysis. Standard curves were performed for FV and for PT using plasma from WT mice (details provided in the Supplementary information file).

Hematological and coagulation tests

FV, PT and aPTT were determined using a STart Max II R coagulometer (Diagnostica Stago S.A.S., Barcelona, Spain), as per the manufacturer's instructions. Cuvettes and metal spheres (Start 4 Cuve, Diagnostica Stago S.A.S., Barcelona, Spain) were used with reagents reconstituted according to the manufacturer's instructions. Measurements included positive and negative controls (System control N/P, Diagnostica Stago S.A.S., Barcelona, Spain).

The measurements were performed in accordance with previously described protocols [22]. Calibration curves were generated using pooled wild-type (WT) plasma (Supplementary Material). Neoplastine CL+ (Diagnostica Stago S.A.S., Barcelona, Spain) was prewarmed to 37 °C before use. FV activity was quantified using 50 µL FV-deficient plasma (Diagnostica Stago S.A.S., Barcelona, Spain) mixed with 50 µL of sample (diluted 1:100 in Owren–Koller buffer [Diagnostica Stago S.A.S., Barcelona, Spain]); mixtures were incubated for 60 seconds, after which 100 µL Neoplastine CL+ were added. Clotting times (s) were converted to FV activity using a calibration curve prepared from serial dilutions of FV-deficient plasma supplemented with pooled normal plasma. Results were reported as a percentage of activity relative to normal pooled plasma, normalized [34,35] and converted to international units per milliliter (IU/mL), assuming 100% FV activity = 1.0 IU/mL. PT was measured using 50 µL of sample at a 1:3 dilution, incubated for 60 seconds, then 100 µL Neoplastine CL+ were added; PT was reported in seconds and as percentages, and INR was calculated as (sample PT / reference PT)^(ISI). For aPTT, a 1:1 mixture of 50 µL plasma and 50 µL PPT Automate was incubated for 180 seconds and then 50 µL of 0.025 M $CaCl_2$ were added to initiate clotting; results were expressed in seconds.

Postmortem studies

Macroscopic and histopathologic assessment

Samples were taken from a variety of organs (skin, skeletal muscle, brain, spinal cord, lymph nodes, heart, lungs, spleen, liver, kidneys, pancreas and gastrointestinal system) and were fixed in 10% neutral buffered formalin for at least 48 hours. In the case of newborns, samples were longitudinally sectioned to facilitate visualization. WT animals without the mutation or any clinical findings were also included as controls to evaluate and compare their histological and immunohistochemical status with that of the deceased animals. The samples were automatically processed (Citadel 2000 Tissue Processor, Thermo Fisher Scientific, Waltham, MA, USA) and embedded in paraffin (HistoStar Embedding Workstation, Thermo Fisher Scientific, Waltham, MA, USA). Four-µm-thick sections were obtained for each case with a microtome (FinesseMe+, Thermo Fisher Scientific, Waltham, MA, USA) and subsequently processed in an automatic slide stainer using hematoxylin-eosin (Gemini AS Automated Slide Stainer, Thermo Fisher Scientific, Waltham, MA, USA). Control and experimental groups are stained under identical conditions with the same batch of reagents.

Immunohistochemical evaluation

The paraffin sections were placed on positively charged microscope slides, deparaffinized with xylene and rehydrated using the Epredia PT Module. Epitopes were retrieved using a heat-induced HIER system (Thermo Fisher Scientific, Waltham, MA, USA). Endogenous peroxidase activity was blocked with 3% hydrogen peroxide in methanol for 30 minutes (Panreac AppliChem ITW Reagents, Barcelona, Spain). Samples were subsequently blocked with 2.5% normal horse serum (RTU) for 1 hour. The sections were then incubated overnight at 4ºC with the primary antibody (Thermo Fisher Scientific, Waltham, MA, USA) (Table 2). Positive and negative controls were included for each batch of sections analyzed. Negative controls were not incubated with

the primary antibody, which was replaced by tris buffered saline (TBS). After incubation, the secondary antibody was added (ImmPRESS® VR Horse AntiRabbit IGG Polymer Kit, Peroxidase; Vector Laboratories, Newark, CA, USA) and incubated for 1 hour at room temperature. The samples were labelled using peroxidase detection system (ImmPACT® NovaRED®Substrate Kit, Peroxidase; Vector Laboratories, Newark, CA, USA) and subsequently counterstained with hematoxylin (Gemini AS Automated Slide Stainer, Thermo Fisher Scientific, Waltham, MA, USA). Control and experimental groups are stained under identical conditions with the same batch of reagents.

To detect the presence of the antigen, intense granular and diffuse cytoplasmic brown labeling were evaluated in combination and considered a positive immunoreaction. A semiquantitative assessment of different specific cells immunolabeled for the specific antigen was performed. Immunolabeled cells were counted in 5 adjacent, non-overlapping fields under a high-power field (HPF) magnification (400×). For FV and thrombin immunoreaction evaluation (macrophages, hepatocytes, neurons, glial cells, endothelial cells) a IHC score (IHCS) from 0 to 3 was assigned to each sample: (0) no presence of immunolabeled cells; (1) 1–10 immunolabeled cells; (2) >10–25 immunolabeled cells; (3) >25 immunolabeled cells.

In addition, the degree of α-smooth muscle actin (α-SMA) immunolabeling (smooth muscle cells, myofibroblasts) in blood vessels was scored as follows: (0) no presence of α-SMA-positive cells in the tunica media; (1) scarce and discontinuous presence of immunoreaction in the tunica media; (2) continuous but thin and incomplete immunoreaction along the tunica media; (3) complete circumferential immunoreaction in the tunica media.

Antibody	Type	Host	Dilution
Anti- thrombin	Polyclonal	Rabbit	1:100
Anti-factor V	Polyclonal	Rabbit	1:100
Anti-α-smooth muscle actin	Monoclonal	Mouse	1:100

Table 2. Antibodies for immunohistochemical study. All antibodies were purchased from Thermo Fisher Scientific.

F5 gene expression study

Embryos and fetal tissues were collected postmortem at various stages of development, as determined by the number of days after detection of the vaginal plug (considered embryonic day 0.5, E0.5). For liver samples, collections were performed at E8, E8.5, E9, E9.5, E10, E11 and E12. For other organs, tissues were collected at E9.5, E10, E11 and E12. Sample collection from embryonic and fetal tissues, as well as from adult animals, were conducted as previously described [36-38]. Total RNA was extracted from the aorta-gonad-mesonephros (AGM) region, head, limbs, somites, yolk sac, gut, and liver using the NZYtech Total RNA Isolation Kit (NZYtech, Ltd., Lisbon, Portugal).

For each tissue and developmental stage, samples were collected in triplicate (n=3 per group) and RNA was quantified using a NanoDrop™ 1000 spectrophotometer (ThermoFisher Scientific, MA, USA). Complementary DNA (cDNA) was generated using the High-capacity cDNA Reverse Transcription Kit (Applied Biosystems, CA USA) for 1 µg of total RNA per sample. Relative transcript abundance was analyzed by qPCR analysis using GoTaq qPCR Master Mix (Promega, WI, USA) in a 7500 fast Real Time PCR thermocycler (Applied Biosystems, ThermoFisher Scientific, MA, USA). qPCR cycle consisted on a holding stage at 50ºC for 2 minutes, followed by denaturation at 95ºC for 10 minutes and 40 cycles at 95ºC for 15 seconds, 60ºC for 1 minute and 72ºC for 30 seconds, and a final 5-minute elongation step at 72ºC followed

by maintenance at 8ºC. Samples were analyzed by the relative gene expression method ($2^{-\Delta Ct}$) and cycle threshold (Ct) values were processed and normalized with respect to the expression of the glyceraldehyde-3-phosphate dehydrogenase (GAPDH) housekeeping gene to estimate the amount of RNA contained in each sample. The samples contained tissue from at least 2 different embryos, were processed in triplicate. Each biological replica was obtained from a different pregnant female. The design of the PCR primers for murine *F5* gene and GAPDH is shown in Table 3.

Gen		Sequence (5´→3´)	Size bp	Gene bank
F5	Forward	GCAGTCACACCACGATCAGA	104	NM_007976.3
	Reverse	TAGGCACTGGGCATCGTTTT		
GAPDH	Forward	CATGGCCTTCCGTGTTCCTA	55	NM_001289726
	Reverse	GCGGCACGTCAGATCCA		

Table 3. qPCR primers.

Statistical analysis

The statistical analysis was conducted using the SPSS 27, v9.4 statistical package (SAS Institute, Cary, NC, USA). The calibration curves for FV and PT were generated using Excel software (Microsoft Office 365) and the graphs were designed using GraphPad Prism 8 software (GraphPad Software, La Jolla, CA, USA). The normality test used for all the parameters was the Shapiro Wilk test. The Levene test was applied to determine whether the variance between the groups was homogeneous. To analyze litter sizes and genotype segregation from heterozygote crosses (Hz×Hz), we performed a chi-square goodness-of-fit (χ^2 GOF) test against the expected Mendelian 1:2:1 distribution (WT:Hz:Hm). The differences in mean coagulometric values between the experimental groups and the control group (WT mice) were assessed using Student's t test. Data was

expressed as mean ± standard deviation. Semi-quantitative immunohistochemical scores were compared using the Mann–Whitney U test.

The relationship between the rate of production of *F5* RNA and the age of embryos and tissues was expressed as mean ± standard deviation and median and range of $2^{-\Delta Ct}$ values. To determine whether there were statistically significant differences between the various embryonic phases with respect to the expression of *F5* RNA, the Krustal Wallis test was used when the normality test was not satisfied; the Levene test was applied to perform the above-mentioned determination. When between-group variance was found not to be homogeneous, a Welch-adjusted ANOVA and the Games-Howell post-hoc test were applied. An ANOVA with Tukey's post-hoc test was used when normality and variance homogeneity were satisfied. Statistical significance was set at a p value < 0.05.

Results

FVFD mutation causes embryonic and postnatal mortality

During the generation of a mouse model carrying Thr1857Met mutation, which produces a mild FV-deficiency phenotype with FV levels of 26% and no spontaneous bleedings [27], an allele with the intended mutation and an allele carrying an indel causing a 4 bp deletion that disrupts the open reading frame of FV (FVFD mutation), was also selected to test the effect of FV protein truncation (as opposed to the single amino acid substitution of Thr1857Met). FVFD mutation generates a protein sharing the first 1851 amino acids with the wild-type sequence, thereby providing a model to determine the physiological role of the amino acids 1852-2224 ablated by the mutation. Cross of heterozygous FVFD animals resulted in an alteration of mendelian inheritance.

The proportion of WT pups was higher the expected (14/24 vs. 6/24) due to a lower proportion of Hz (6/24) and Hm (4/24) pups, which suggest embryonic or fetal mortality of Hz and Hm individuals. Based on the χ^2 GOF analysis—and considering the expected 1:2:1 distribution for heterozygote crosses (WT, Hz, Hm)—we obtained $\chi^2 = 14.33$, df = 2, p = 0.0008. Tree of the four Hm pups died shortly after delivery showing signs of congestion and severe hematomas. The survivor Hm individual developed to weaning (day 21, hereinafter the young Hm individual) and subsequently died without any visible signs of bleeding. No viable Hm animals were obtained for the coagulometric assays. On ear punching, Hz individuals presented with longer bleeding times than WT individuals.

FVFD mutation alters coagulometric pattern

An analysis was made of FV, aPTT and PT levels in mice. Individuals had a mean weight of 20.62 ± 3.14 grams. The FV values obtained (Fig. 1A) were expressed as IU/mL (or % activity). Mean FV activity was 1.00 UI/mL ± 0.13 (107.50% ± 14.21) in WT individuals; and 0.22 IU/mL ± 0.09 (21.53% ± 9.26) in Hz individuals. A normal distribution yet dissimilar variances were observed between the groups. Welch`s Student's t test found statistically significant differences between WT and Hz group ($p<0.001$).

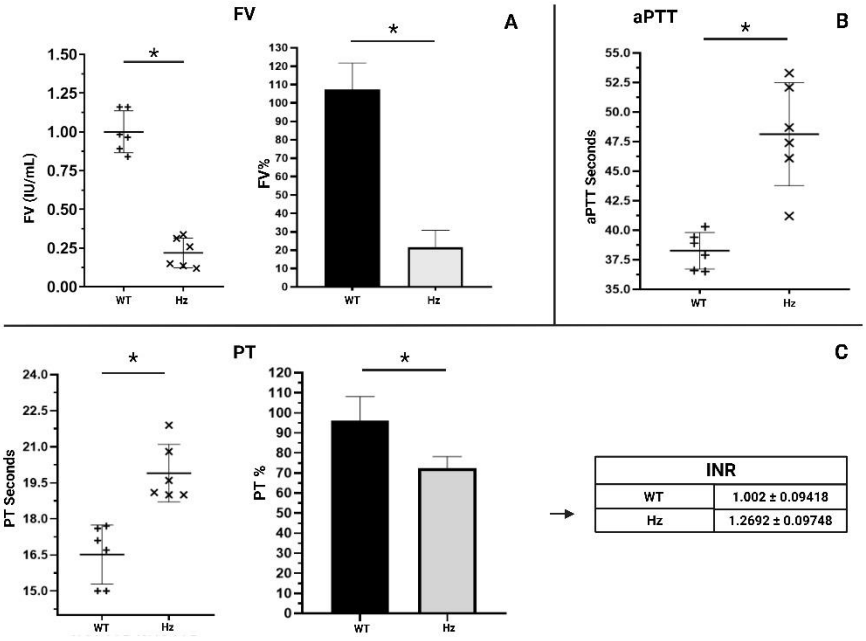

Fig. 1. Coagulometric measurements for WT and Hz groups. (A) FV activity expressed in UI/mL and percentage (n=6). (B) aPTT expressed in seconds (n=6). (C) PT expressed in seconds, percentage and INR (n=6). Calibration curves were generated using pooled wild-type (WT) plasma. The data are expressed as mean ± standard deviation. *p<0.05 according to Student's t test. Abbreviations: FV, factor V; Hz, heterozygous; INR, international normalized ratio; WT, wild type.

Mean aPTT, expressed as time to clot formation (seconds), was 38.26 seconds ± 1.53 in WT animals; and 48.13 seconds ± 4.37 in Hz animals (Fig. 1B). Normal distribution and identical variances were observed between the groups. Student's t test revealed statistically significant differences between the WT group and the Hz group ($p<0.001$).

Mean PT, expressed as time to clot formation (seconds) and percentages on the standard curves based on plasma pool of WT animals, was 16.51 seconds ± 1.22 (96.24% ± 11.87) in WT animals; and 19.90 seconds ± 1.19 (72.36% ± 5.85) in Hz animals (Fig. 1C). A normal distribution and similar variances were observed between the groups. Student's t test revealed statistically significant differences between WT and

Hz individuals ($p<0.001$). INR was also calculated for each group based on the plasma pool of WT animals, with a PT value of 17 seconds and an ISI of 1.27. INR was 1.002 ± 0.09418 for WT individuals; and 1.2692 ± 0.09748 for Hz individuals.

Post-mortem analyses of Hm FVFD individuals

The main finding of the post-mortem study of newborn Hm animals was generalized congestion in the skin and internal organs. One of the dead Hm neonates also exhibited extensive erythematous areas, as well as multifocal hemorrhages in the head, the neck, parts of the thoracic region and the anterior limbs (Figs. 2A and 2B**)**. The young Hm individual exhibited submeningeal hemorrhages in the cranial vault, mainly in the frontal and interparietal sutures, which extended into the parenchyma (Figs. 2C and 2D).

Histologically, dead Hm newborn animals only exhibited blood vessel congestion and perivascular extravasation of erythrocytes. The young Hm individual exhibited multifocal hemorrhages in the perivascular spaces of the brain. Extensive hemorrhagic areas were also evident in meninges and cerebral ventricles (Figs. 2E and 2F).

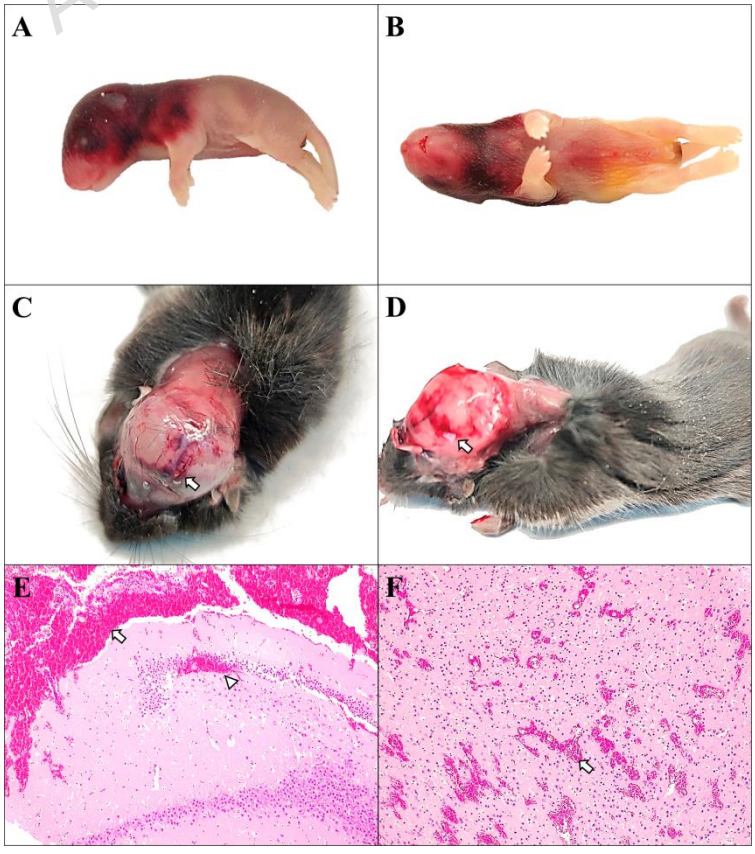

Fig. 2. Main pathological findings in newborn Hm individuals (A, B) and in the young Hm individual (C, F). (A, B) Extensive light red erythematous area with bright red multifocal hemorrhages, encompassing the skull, eyes, submandibular and cervical areas, anterior aspect of the thoracic region and proximal anterior limbs. (C, D) Sub meningeal multifocal hemorrhagic areas, mainly at the frontal and interparietal sutures (arrows). (E) Extensive hemorrhagic areas adjacent to the molecular layer of the hippocampal dentate gyrus (arrow) and multifocal hemorrhages occupying the molecular layer of the dentate gyrus (arrowhead). The cells comprising the molecular and polymorphic layers of the dentate gyrus present with cytoplasmic vacuolation. H&E stain, 10x. (F) Perivascular multifocal hemorrhages located in the neuropil of the thalamus (arrow); H&E stain, 10x. Abbreviations: Hm, homozygous.

An immunohistochemical analysis of the expression of thrombin, FV and α-SMA was conducted to compare the dead Hm newborns and the young Hm individual with respect to WT animals. The *U*-Mann-Whitney analysis (M-W test) revealed significant differences between Hm and wild-type WT animals, highlighting differences in thrombin distribution in liver (M-W test: $p < 0{,}0001$) and in α-SMA distribution in brain, liver and heart (M-W test: $p < 0{,}0001$). Minimal signal was detected for thrombin immunolabeling in some of the studied organs of newborn Hm animals: in the brain, minimal immunolabeling was observed in the cytoplasm of the neurons and glial cells, close to the subarachnoid space (IHCS mean = 0.53; 95% confidence interval (CI): 0.24-0.82) (Fig. 3A); in the liver, minimal immunostaining was detected in the hepatocyte cytoplasm and the Kupffer cells (IHCS mean = 0.60; 95% CI: 0.32-0.88). Newborn WT animals presented moderate immunolabeling in the brain, particulary in the cytoplasm of the neurons and glial cells, close to the subarachnoid space (IHCS mean = 2.4; 95% CI: 1.29-3.00) (Fig. 3B**).** Moreover, these animals exhibited mild immunolabeling in the hepatocytes cytoplasm and the Kupffer cells of the liver (IHCS mean = 0.80; 95% CI: 0.25-1.36).

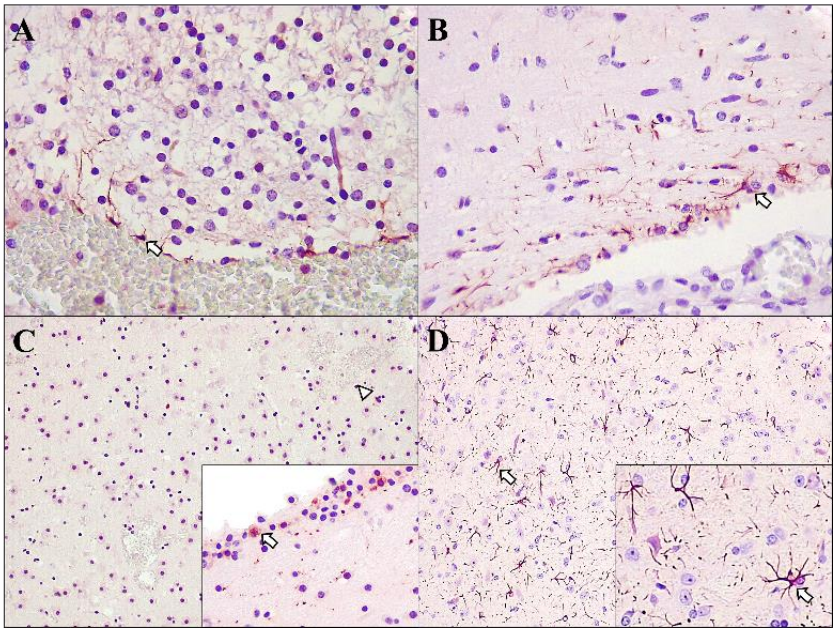

Fig. 3. Distribution and location of thrombin immunolabeling in the brain cells of newborn Hm mice (A) and the young Hm individual (C), as seen by immunohistochemistry analysis. Images from newborn WT animals (no mutation) (B) and adult WT animals (no mutation) (D). (A) Minimal immunolabeling in the cytoplasmic projections of neurons and glial cells (arrow) close to the subarachnoid space, which was full of erythrocytes; rabbit polyclonal anti-thrombin antibody, 40x. (B) Moderate immunolabeling in the cytoplasmic projections of neurons and glial cells (arrow) close to the subarachnoid space; rabbit polyclonal anti-thrombin antibody, 40x. (C) No immunolabeling was observed in the cytoplasm of neurons and glial cells within the thalamus, adjacent to perivascular hemorrhagic areas (arrowhead); rabbit polyclonal anti-thrombin antibody, 20x. Inset: minimal immunolabeling in the cytoplasm of the glial cells close to the ependyma, 40x. (D) Intense immunolabeling in the dendritic projections of the neuronal cytoplasm and glial cells within the thalamus (arrow); rabbit polyclonal anti-thrombin antibody, 20x. Inset: intense immunolabeling in the dendritic cytoplasmic projections (arrow), 40x. Abbreviations: Hm, homozygous; WT, wild type.

The young Hm individual did not exhibit a positive thrombin immunolabeling in any organ, except for the brain, where minimal granular immunolabeling was detected in the cytoplasm of the neurons, close to the ependyma (IHCS mean = 0.80; 95% CI: 0.25-1.36) (Fig. 3C). No immunolabeling was visible adjacent to the brain hemorrhages observed. On the other hand, young WT animals exhibited an intensely positive immunolabeling in the brain, at the level of the dendritic cytoplasmic projections of the glia and neurons, mainly in myelin-rich and perivascular areas (IHCS mean = 2.60; 95% CI: 1.92-3.00) (Fig. 3D**)**.

Regarding FV presence, no immunolabeling signal was detected in newborn Hm animals immunolabeling signaling the studied organs, except for the liver where slight-to-moderate cytoplasmic signal was detected in hepatocytes and Kupffer cells (IHCS mean = 1.53; 95% CI: 1.18-1.89) (Fig. 4A). Newborn WT individuals also exhibited a mild-to-moderate immunolabeling in liver (IHCS mean = 2.40; 95% CI: 1.72-3.00) (Fig. 4B). No significant immunolabeling was detected in any of the analyzed organs of the young Hm individual except for the liver (IHCS mean = 1.20; 95% CI: 0.65-1.76). Moreover, young WT animals exhibited a mild immunolabeling signal in the liver (IHCS mean = 1.40; 95% CI: 0.72-2.08) and the brain, particularly in the cytoplasm of neurons, with intense staining in Nissl bodies (IHCS mean = 0.80; 95% CI: 0.25-1.36) (Figs. 4C and 4D).

Although in an unspecific and diffuse manner, staining for thrombin and FV was observed in various structures such as the respiratory epithelium of the bronchi and bronchioles, the renal tubules, the spleen, the glandular structures of the gastrointestinal system and the pancreas, as well as in the skeletal, cardiac and smooth musculature.

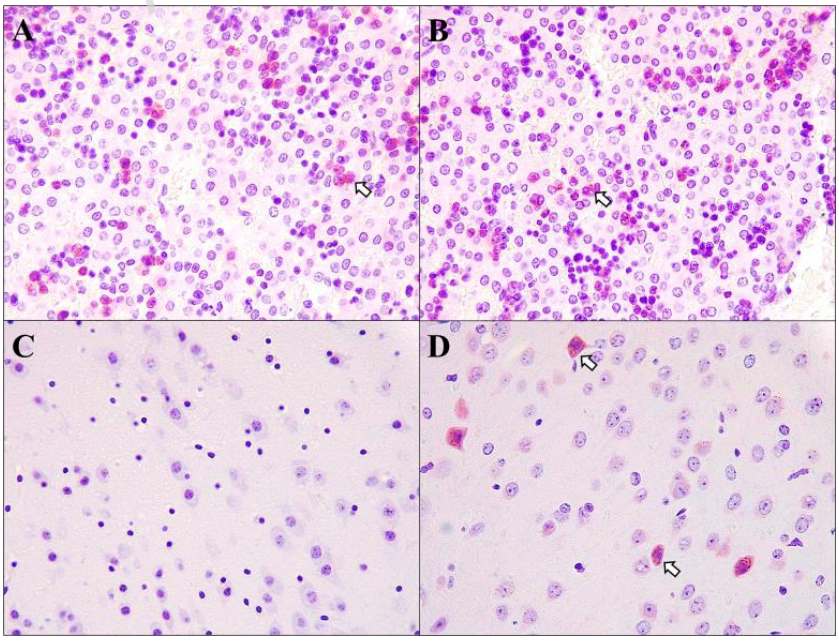

Fig. 4. Distribution and location of factor V in liver (A, B) and brain cells (C, D) of newborn Hm individuals (A) and of the young Hm individual (C) as seen by immunohistochemistry analysis. Images from newborn WT animals (B) and adult WT animals are included (D). (A) Moderate diffuse immunolabeling in the cytoplasm of hepatocytes and the Kupffer cells (arrow); rabbit polyclonal anti-FV antibody, 40x. (B) Moderate granular and diffuse immunolabeling in the cytoplasm of hepatocytes and the Kupffer cells (arrow); rabbit polyclonal anti-FV antibody, 40x. (C) No immunolabeling in the neurons' cytoplasm; rabbit polyclonal anti-FV antibody, 40x. (D) Moderate granular and diffuse immunolabeling in the neuronal cytoplasm (arrow); rabbit polyclonal anti-thrombin antibody, 40x. Abbreviations: Hm, homozygous; WT, wild type.

Regarding α-SMA analysis, newborn Hm animals showed a faint immunolabeling in the cells of the centrilobular vein walls and in the vessels of the hepatic portal space (IHCS mean = 0.87; 95% CI: 0.51-1.22) (Fig. 5A). The same finding was observed at the level of the heart, with a slight immunolabeling in the myocardial vessels (IHCS mean = 1.07; 95% CI: 0.68-1.46) (Fig. 5C). This contrasts with the intensely positive immunolabeling of the same vascular structures in liver (IHCS mean = 2.80; 95% CI: 2.50-3.00) and heart (IHCS mean = 2.70; 95% CI: 2.35-3.00) in WT individuals, where vascular walls were found to be thicker than in Hm animals (Figs. 5B and 5D).

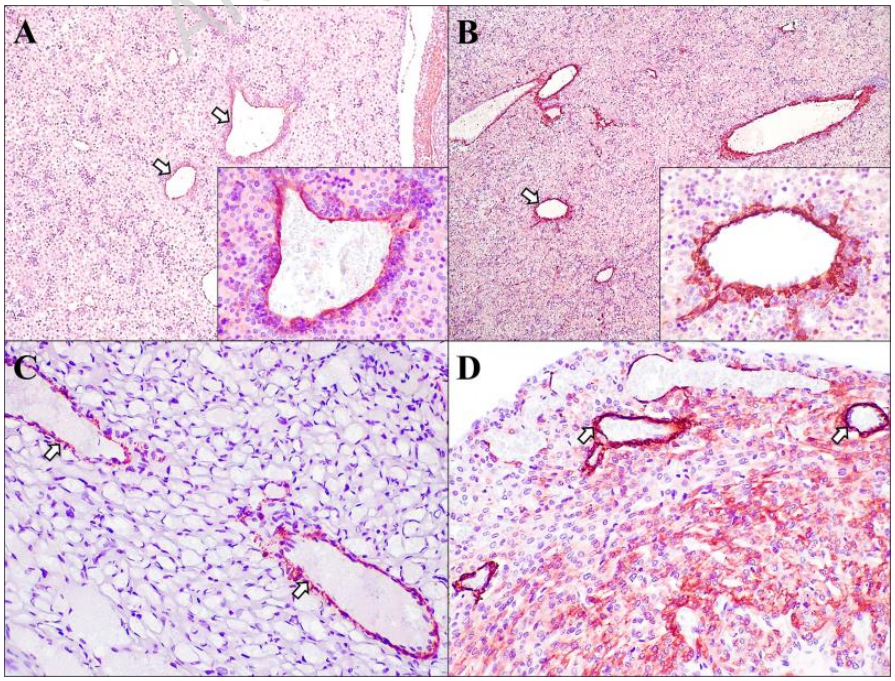

Fig. 5. Immunolabeling of blood vessels in the presence of α-SMA in the liver (A, B) and the heart (C, D) of newborn Hm individuals (A, C), as seen by

immunohistochemistry analysis. Images from newborn WT animals are included (B, D). (A) Slight immunolabeling in centrilobular veins and in the vessels of the portal space (arrow); mouse anti-α-SMA monoclonal antibody, 4x. Inset: slight immunostaining of the cells of the centrilobular vein wall, 40x. (B) Intense immunolabeling in the centrilobular veins and in the vessels of the portal space (arrow); mouse anti-α-SMA monoclonal antibody, 4x. Inset: intense immunostaining of the cells of the centrilobular vein walls, showing a thickened vascular wall, 40x. (C) Slight immunolabeling in the myocardial vessels; anti-α-SMA monoclonal antibody in the mouse, 20x. (D) Intense immunolabeling in myocardial vessels and moderate immunolabeling in cardiomyocytes; mouse anti-α-SMA monoclonal antibody, 20x. Abbreviations: Hm, homozygous; WT, wild type.

The young Hm individual exhibited a reduced expression of α-SMA on the walls of the centrilobular vein and in the hepatic artery (Figs. 6A and 6B) while WT individuals displayed an intense expression in the portal vein, the hepatic artery and the centrilobular vein. In addition, a very intense and homogeneous immunolabeling was observed in the myocardial vessels of WT mice, while the young Hm individual exhibited a discontinuous immunolabeling on the myocardial vessel wall (Figs. 6C and 6D).

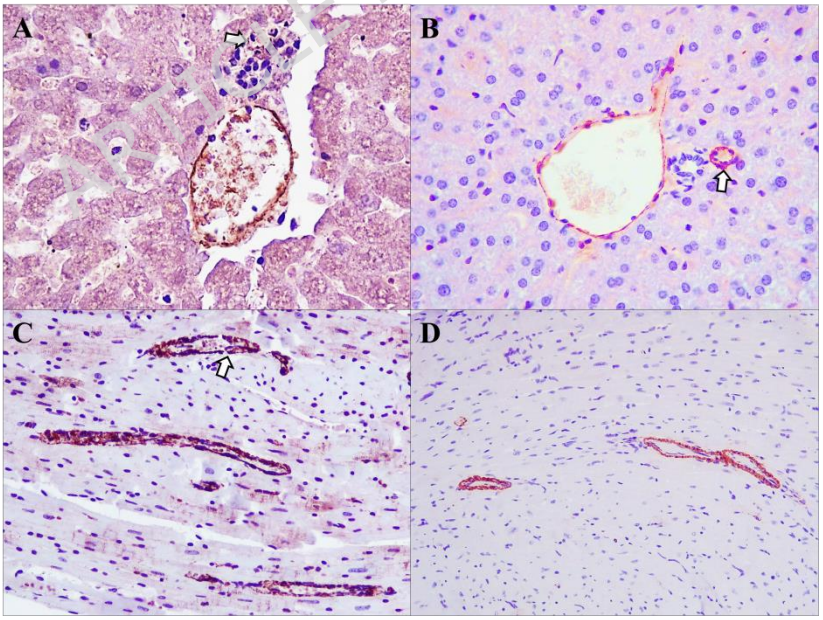

Fig. 6. Immunolabeling of blood vessels in the presence of α-SMA in the liver (A, B) and the heart (C, D) of the young Hm individual (A, C) as seen by immunohistochemistry analysis. Images from WT animals (no mutation) (B, D). (A) Interrupted immunolabeling in the portal vein and attenuated response in the hepatic artery (arrow); mouse anti-α-SMA monoclonal antibody, 40x. (B) Homogeneous immunolabeling in the portal vein and intense immunolabeling in the hepatic artery (arrow); anti-α-

SMA monoclonal antibody in the mouse, 40x. (C) Interrupted immunolabeling in the myocardial vessels (arrow); mouse anti-α-SMA monoclonal antibody, 20x. (D) Homogeneous immunolabeling in the myocardial vessels; mouse anti-α-SMA monoclonal antibody, 20x. Abbreviations: Hm, homozygous; WT, wild type.

Analysis of *F5* expression during embryogenesis

The spatiotemporal expression of the *F5* mRNA was first evaluated by qPCR of the *F5* gene in mouse embryos at different stages of development (E8, E8.5, E9, E9.5, E10, E11 and E12) and in the adult mouse liver (Fig. 7). In mice, the liver emerges at stage E9 and megakaryocytes at E7.5. Subsequently, several embryonic tissues were analyzed (AGM region, head, heart, limb, somites, yolk sack, gut and liver) at the following stages: E9.5, E10, E11 and E12 (Figs. 8 and 9).

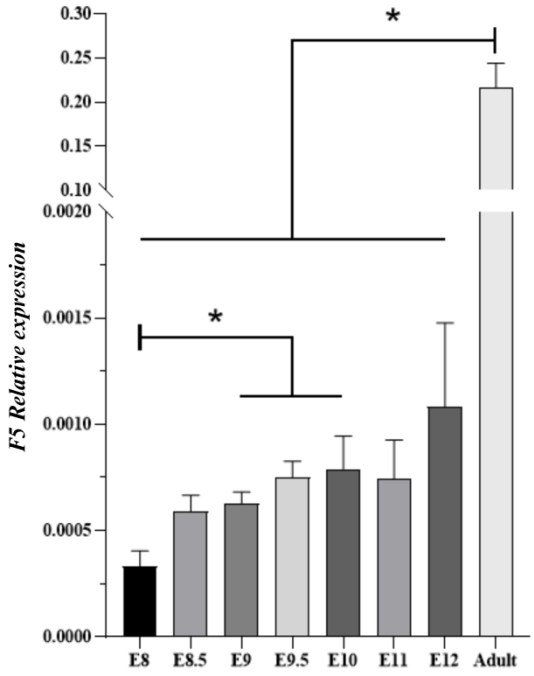

Fig. 7. Relative expression of the *F5* gene (n=3-4) at various stages of embryonic development and in adult mouse liver (mean ± standard deviation). Significant differences are indicated by lines and asterisks (*p<0.05) according to Welch's ANOVA. Abbreviation: E, embryonic stage.

A progressively greater expression of the *F5* gene was found from earlier stages of development until the adult stage, where significantly higher values were observed. The mean values obtained, expressed as mean ± standard deviation, reflected a progressively greater expression over the course of development. At stage E8 *F5* gene expression was 0.00033 ± 0.00007, while at stage E8.5 it increased to 0.00059 ± 0.00007. In the following stages, values kept increasing to reach 0.00063 ± 0.00005 at stage E9, 0.00075 ± 0.00008 at stage E9.5, and 0.00079 ± 0.00015 at stage E10. Mean values in the more advanced developmental stages (E11 and E12) were 0.00074 ± 0.00018 and 0.00108 ± 0.00039, respectively. Finally, in the adult stage, *F5* gene expression reached significantly higher values, 0.21603 ± 0.02818.

To evaluate the significance of the varying expression levels observed over the different stages of embryogenesis and given that the Levene test indicated a lack of homogeneity among the variances ($p<0.05$), it was decided to conduct Welch's ANOVA. The post-hoc test revealed significant differences in *F5* gene expression between several stages of embryonic development. Particularly significant differences were found between stages E8 and E9 ($p=0.044$), E8 and E9.5 ($p=0.019$), and E8 and E10 ($p=0.040$). In addition, significant differences were observed between the adult stage and stages E8 to E12 ($p=0.025$).

Overall, these results demonstrated a progressive increase of *F5* gene expression from the earlier stages of development to the adult stage, where significantly higher values were achieved.

Regarding *F5* expression dynamics in specific organs and tissues, no statistically significant differences were observed between stages in AGM region, head, heart, limbs, somites and digestive tract. In the yolk sac, the highest expression level was observed at stage E9.5, gradually decreasing until stage E12 (0.0035753 to 0.0005425). Statistically significant differences were observed between stages E9.5 and E11 ($p=0.014$), E9.5 and E12 ($p=0.014$), E10 and E11 ($p=0.014$), and E10 and E12 ($p=0.014$). In the liver, a significant increase was observed in *F5* gene expression until stage E12 (0.0012 ± 0.000088 to 0.01053 ± 0.00175). Statistically significant differences were found between E12 and E9.5, E10 and E11, with $p<0.001$ in all cases (Fig. 8).

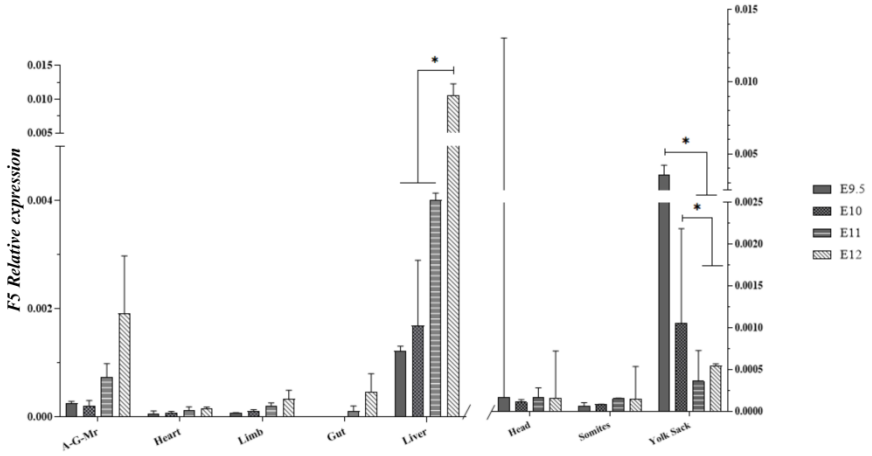

Fig. 8. Relative expression of the *F5* gene ($2^{-\Delta Ct}$) across different tissues at stages E9.5, E10, E11 and E12. On the left of the graph, values are represented as mean ± standard deviation (SD), whereas on the right, they are shown as median and range. Significant differences are indicated by lines and asterisks (*p<0.05) according to Welch's ANOVA or Krustal Wallis. Abbreviations: AGM, aorta-gonad-mesonephros region.

Differences in the expression levels of various organs were analyzed at each stage of embryonic development. At stage E9.5 (Fig. 9A), the highest relative abundance was observed in the yolk sac, being significantly higher compared with that of heart, limbs and somites (p=0.006, p=0.012 and p=0.015 respectively). The liver was the organ showing the second highest relative abundance, being significantly higher compared with heart (p=0.01), limbs (p=0.021) somites (p=0.025), heart and head (p=0.048).

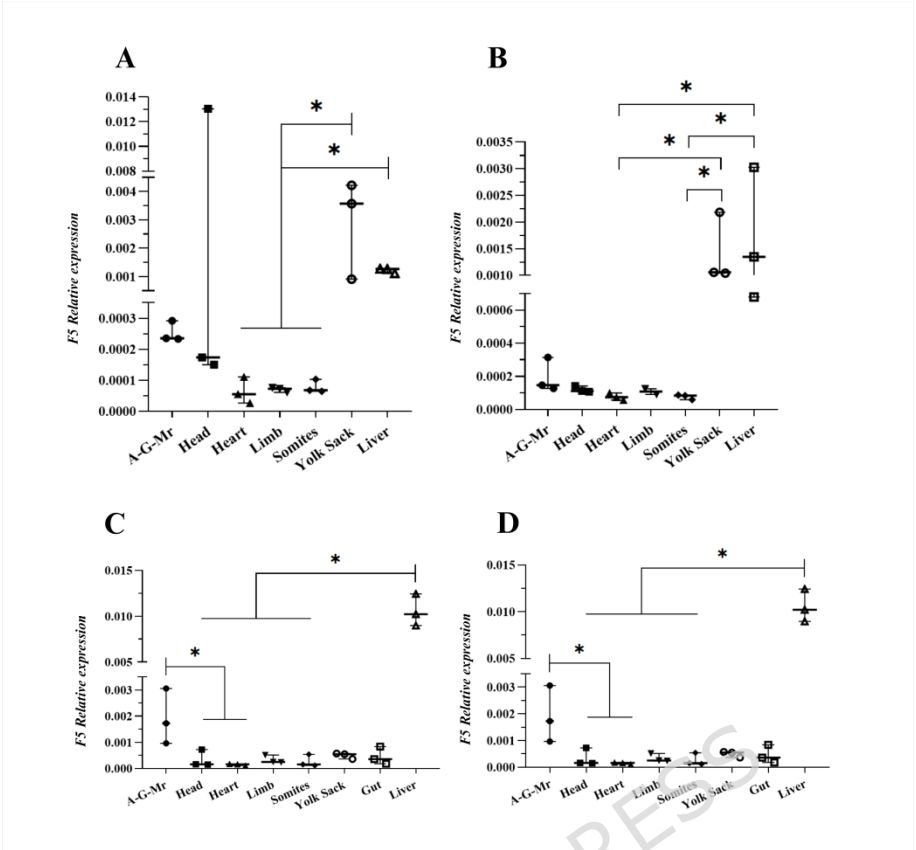

Fig. 9. Relative expression of the *F5* gene ($2^{-\Delta Ct}$) across different tissues at the various stages. (A) Stage E9.5 (median and range). (B) Stage E10 (median and range). (C) Stage E11 (mean ± SD). (D) Stage E12 (median and range). Significant differences are indicated by lines and asterisks (*$p<0.05$) according to Welch's ANOVA or Krustal Wallis. Abbreviations: AGM, aorta-gonad-mesonephros region.

At stage E10 (Fig. 9B), significant differences were observed in *F5* mRNA relative abundance in liver compared to heart and somites ($p=0.004$ in both cases). *F5* mRNA relative abundance was also significantly higher in yolk sac compared to heart and somites ($p=0.005$ in both cases). At stage E11 (Fig. 9C), *F5* relative mRNA abundance was higher in liver compared to other organs analyzed ($p<0.001$) and significant differences were observed between the AGM region and the head, the heart, the limbs, somites and the digestive tract.

Finally, at stage E12 (Fig. 9D), the liver was the organ showing the highest *F5* relative mRNA abundance. Significant differences were also observed between AGM region (the organ showing the second highest *F5* relative mRNA abundance) compared

to heart and head. All the measurements conducted can be found in the Supplementary information file.

Discussion

The CRISPR/*Cas*9 system has emerged as a key tool to generate animal and cell models for various diseases [39,40]. The present study provides an analysis of the phenotype in a mouse model producing a truncated FV protein.

Mutations resulting in protein truncation often result in more severe phenotypes than those involving amino acid substitutions [41,42]. In hemophilia A and B, frame disrupting account for a significant percentage of the mutations described and give rise to severe phenotypes [43,44]. Similarly, in FV deficiency very severe disease phenotypes (<1% FV levels) have been described as a result of FV truncation [7], which represents 15% of all the mutations leading to FV-deficiency described so far [7,8], most of them located in exon 13. The phenotypic consequences of FV truncation in a downstream region (exon 18), a phylogenetically conserved region where single amino acid substitution are known to cause coagulation deficits, were unknown [27].

Knockout models for FV deficiency have been generated both in mice and in the zebra fish, with stop codons being identified in various regions of the FV protein [24,25]. Cui et al. [24] succeeded in generating a mouse model with a frameshift mutation in Hm animals that gave rise to embryonic resorption during embryogenesis as a result of a severe FV (and therefore thrombin) deficiency. Previous studies have also demonstrated that, in FV-deficient mice, even a very small amount of FV may be sufficient to avert the severe consequences of severe FV deficiency over the course of embryogenesis [26]. In a recent study by our research group [27], the introduction of a single amino acid substitution resulted in a mild disease phenotype. In this case Hm

individuals were viable, showing that embryonic alterations can be prevented if FV retains some functionality.

FVFD model displayed a clear alteration of coagulometric parameters. Whereas WT individuals exhibited FV levels approaching 100%, in line with previous reports [23], and PT and aPTT levels were within the normal ranges [45]. Hz animals for FVFD showed a reduction in FV levels similar to those of Hm individuals with a mild phenotype of FV deficiency [9,46]. This suggest that the truncated FV protein affect the functionality or bioavailability of the WT FV also produced by the Hz individuals, in line with observations in humans, where Hz individuals display a reduction of FV plasma levels to around 20% [11]. A previous study by our group [47] also observed such a drop in circulating levels of FV in the parents of a patient with severe FV deficiency. However, in this human study, PT and aPTT levels were not significantly decreased, probably because of the activity of other coagulation factors or by the production of functional FV thanks to the heterozygous condition [9,47]. The detrimental effects of the truncated protein over the functionality of the WT protein may be caused by a conformational change in FV truncated protein preventing proper functioning of the C domains responsible for binding to membrane lipids and to prothrombinase complex [48]. This could result in a critical functional decrease in the coagulation activity of Hz animals.

An analysis of histological lesions in deceased Hm animals revealed that the integrity of the tissues was compromised because of multiple autolytic processes [49]. In spite of that, hemorrhages were observed in several body parts of both newborn and young individuals, a finding also commonly reported in humans, both in terms of clinical signs and their sequelae [7,50].

It has been reported that hemostasis and its various components, including FV, play a crucial role during embryonic development. They modulate cell activity through receptor-dependent signaling pathways, both inside and around the embryonic vasculature. They also participate in essential processes such as angiogenesis and vasculogenesis, cell differentiation and tissue remodeling [51,52].

Given the limited number of reports on human miscarriages in the literature on FV-deficiency, Naderi et al. [53] described that miscarriages in human Hz mothers are attributable to the deficiency. This was the case in our FVFD model, where several litters of an Hz mother only resulted in 4 Hm individuals none of which survived over the long term. In humans, the prevalence of FV-deficiency is calculated based on live births, which means that possible miscarriages or instances of embryonic resorption may go unaccounted for [3].

As reported by Cui et al. [24] it is half way through embryonic development (E11) when most instances of embryonic resorption are observed in mice. This study indicates that the onset of embryonic development is characterized by high FV levels in the mouse's yolk sac. The yolk sac precedes the development of the placenta and provides the embryo with nutrients and oxygen. It is a richly vascularized organ and it plays an important functional role in embryonic development [54]. It has been shown that it is chiefly the endoderm that is responsible for producing the coagulation factors. This finding, which confirms our results, is in line with the fact that, in humans, the yolk sac is one of the sources of FV [55]. This could be one of the reasons for embryonic resorption and for the low birth rates observed among Hm animals. Our data indicates descriptive developmental trends in *F5* transcripts (AGM and liver increasing, yolk sac decreasing from E9.5 to E12.5). While informative, these transcript patterns are insufficient to establish causality, and additional studies will be required.

Our study shows that expression of the *F5* gene in the liver increases progressively until the adult stage. However, this finding is not borne out by immunohistochemical studies. The liver is responsible for most of the FV generated in the body [7,56]. The progressive increase in FV levels observed until the adult stage may be taken to suggest that it plays a significant role in the maturation of the hemostatic system during the development of the mouse. However, the immune expression of FV in the liver was moderate, both in newborn and adult animals. This could indicate that most FV is either not stored in that organ or it is instead released to the bloodstream, or it is stored in hepatocytes but in an immature form, as is the case of other vitamin K-dependent coagulation factors [57,58].

This still unresolved question is further complicated by the intriguing immunohistochemical finding that FV levels appear to be higher in newborn than in adult WT animals. This could indicate that during the neonatal period, FV is actively involved in various vascular and life-sustaining processes, whereas in the adult stage its function could be that of a defense mechanism against vascular damage through hemostasis [3,24,59].

A comparison of the immune expression of FV in WT and FVFD Hm animals shows higher intensity in WT individuals, which suggests normal expression and function of the protein. Nonetheless, expression of FV in FVFD Hm individuals has been shown to be attenuated or even undetectable, which may be indicative of insufficient production levels; a conformational change hindering its function or its detection; or even a decrease in the stability of the protein [7,60]. No significant differences were found in the liver between WT and FVFD animals, which would appear to support our assumption that FV is not stored in the hepatocyte or that it exists in liver cells only in an immature form. With respect to FV expression in the nervous

system —its presence has been reported in Schwann cells [61]— FVFD animals showing a decreased immune expression in the neural cytoplasm. The importance of FV in embryonic development does not lie exclusively in its ability to regulate vascular or early developmental processes, but also in its interaction with protease-activated receptors (PARs), particularly PAR1, as it contributes to regulating numerous key processes such as angiogenesis and tissue remodeling [28,31]. It is well known that these receptors are activated by thrombin whose expression is FVa-dependent [1]. Moreover, it is believed that FV-deficient animals are characterized by an impaired development of PAR1 receptors, which gives rise to vascular abnormalities, inadequate vascular development and even miscarriages over the course of embryogenesis [24,28,31].

Thrombin expression largely depends on the animals' physiological condition and, in the absence of vascular damage, it is rarely detected in organs, being present mainly in the blood [62]. Nevertheless, immunohistochemical studies revealed statistically significant differences between WT and FVFD Hm animals, particularly in the brain, where an intense immune expression against thrombin was observed in WT adults, which contrasts with an almost undetectable expression in FVFD animals. This finding is compatible with the absence of an immune expression for FV in the brain of FVFD Hm animals, suggesting that the main cause of bleeding in these individuals is the absence of thrombin production resulting from an insufficient production of FV, which prevents the proper functioning of the clotting cascade in the event of a lesion. At the same time, the role of thrombin in the central nervous system is now clearly understood. This enzyme, which is expressed locally in neural cells and astrocytes, plays a dual role with either a cytoprotective or a harmful role depending on its concentration. Thrombin regulation is key in the context of neurological lesions or

conditions as it may act as a mediator of inflammation and cell death, affecting cell integrity and influencing the progression of neurological disorders [63].

Lastly, an analysis was conducted of the immune expression of α-actin, which regulates vascular tone and function as well as smooth muscle integrity in large blood vessels. A report in the literature described a decrease in α-actin expression in hemophilic mice [64,65]. This study demonstrated a considerably decreased α-actin protein expression in the liver and the heart of FVFD animals as compared with WT animals, which exhibited thicker vessel walls. In line with a relationship between thrombin and α-actin, both proteins co-localize, being related to PAR receptors [66]. This may indicate that, in the same way as there exists a relationship between FVIII activity and α-actin, FV could exert a direct influence on α-actin expression, a hypothesis that needs to be confirmed by further research.

The homozygous cohort comprised three newborns and a single 21-day individual, which limits statistical inference; in accordance with the 3Rs (Replacement, Reduction, Refinement), we did not expand breeding and considered this sample sufficient to document the phenotype while avoiding additional animal suffering. The analysis of FV, thrombin, and smooth muscle α-actin by immunohistochemistry was conducted qualitatively. Future studies incorporating quantitative techniques are recommended to confirm and extend the current findings. In particular, future work will include quantitative protein assays (e.g., by Western blot/ELISA) of the analyzed parameters.

Conclusion

FV is not only a key protein in secondary hemostasis, but it also plays an important role in the formation, maturation and stabilization of blood vessels over the course of embryonic development. A severe deficiency in FV has a highly deleterious effect on different developmental mechanisms and may result in miscarriages or even in embryonic resorption as has been shown in knockout animal models. The integrated coagulometric, histopathological, immunohistochemical and gene expression data presented here provide additional mechanistic insight into how FV supports embryonic vascular development through thrombin-dependent signalling and α-SMA, and illustrate the developmental consequences of its deficiency in the context of congenital bleeding disorders.

Acknowledgements

The authors would like to thank Benedicto Jerónimo, supervisor of the animal facility, for his care for the safety and welfare of the animals. We thank the technical staff at CABD, Tamara Garcia-Leal, Ana Franco, and Candida Mateos, for their support with embryo collection and animal husbandry. We would also like to thank the genomics unit, CAI of biological techniques, of the Complutense University of Madrid, for their work on the Sanger sequencing of the samples.

Competing interests

The authors declare that they have no competing interests. AL, JADPM, LR, AMB, PBA, and LGB, have a mouse model, deficient in factor V, protected by Spanish patent (Ref. ES2948817B2). Holders: Complutense University of Madrid, and Superior Council for Scientific Research. Spain. Official Bulletin of Industrial Property (21-02-2024) Volume 2: Inventions. p. 8. Available in: https://sede.oepm.gob.es/bopiweb/descargaPublicaciones/formBusqueda.action.

Data availability

The data generated during and/or analyzed during the current study are available from the corresponding author (Antonio Liras) on reasonable request, and in the Supplementary information file.

Ethics approval statement

The study was conducted in compliance with Royal Decree 53/2013 and Directive 2010/63/EU. All procedures used were approved by the School of Veterinary Medicine of the Complutense University of Madrid, the Ethics Committees on Animal Experimentation of the Complutense University, and the Madrid Regional Government (PROEX 040/17 and PROEX 358.4/21).

Funding

This research was funded by the Association for Research and Cure of Factor V deficiency (ASDEFAV), grant number ASDEFAV/2021-25; the Complutense University of Madrid and Banco Santander, grant number CT63/19-CT64/19; the Spanish Ministry of Science and Innovation, grant number PID2020-117501RB-I00; the Community of Madrid, grant number CT85/23; Spanish María de Maeztu Unit of Excellence, grant CEX-2020-001088-M to the CABD, and by Regional Government of Andalusia, Department of Innovation (PAI-BIO-295).

References

1. Barcellona, D. & Marongiu, F. The hemostatic system. 1st Part. *J. Pediatr. Neonat. Individ. Med.* **9**, e090106; 10.7363/090106 (2020).
2. Versteeg, H.H., Heemskerk, J.W.M., Levi, M. & Reitsma, P.H. New fundamentals in hemostasis. *Physiol. Rev.* **93**, 327–358; 10.1152/physrev.00016.2011 (2013).
3. De Pablo-Moreno, J.A., Miguel-Batuecas, A., De Sancha, M. & Liras, A. The magic of proteases: from a procoagulant and anticoagulant factor V to an equitable treatment of its inherited deficiency. *Int. J. Mol. Sci.* **24**, 6243; 10.3390/ijms24076243 (2023).
4. Mohapatra, A.K., Todaro, A.M. & Castoldi, E. Factor V variants in bleeding and thrombosis. *Res. Pract. Thromb. Haemost.* **8**, 102330; 10.1016/j.rpth.2024.102330 (2024).

5. Asselta, R. & Peyvandi, F. Factor V deficiency. *Semin. Thromb. Hemost.* **35**, 382–389; 10.1055/s-0029-1225760 (2009).
6. Huang, J.N. & Koerper, M.A. Factor V deficiency: a concise review. *Haemophilia* **14**, 1164–1169; 10.1111/j.1365-2516.2008.01785.x (2008).
7. Tabibian, S. *et al.* A comprehensive overview of coagulation factor V and congenital factor V deficiency. *Semin. Thromb. Hemost.* **45**, 523–543; 10.1055/s-0039-1687906 (2019).
8. The Human Gene Mutation Database at the Institute of Medical Genetics in Cardiff (HGMD). *The human gene mutation database at the Institute of Medical Genetics in Cardiff* http://www.hgmd.cf.ac.uk/ac/index.php (2025)
9. Moret, A. *et al.* Next generation sequencing in bleeding disorders: two novel variants in the F5 gene (Valencia-1 and Valencia-2) associated with mild factor V deficiency. *J. Thromb. Thrombolysis* **48**, 674–678; 10.1007/s11239-019-01911-z (2019).
10. Caudill, J.S. *et al.* Severe coagulation factor V deficiency associated with an interstitial deletion of chromosome 1q. *J. Thromb. Haemost.* **5**, 626–628; 10.1111/j.1538-7836.2007.02363.x (2007).
11. Guasch, J.F. *et al.* Severe coagulation factor V deficiency caused by a 4 bp deletion in the factor V gene. *Br. J. Haematol.* **101**, 32–39; 10.1046/j.1365-2141.1998.00664.x (1998).
12. Holmberg, L., Henriksson, P., Ekelund, H. & Åstedt, B. Coagulation in the human fetus. *J. Pediatr.* **85**, 860–864; 10.1016/S0022-3476(74)80361-6 (1974).
13. Poralla, C. *et al.* The coagulation system of extremely preterm infants: influence of perinatal risk factors on coagulation. *J. Perinatol.* **32**, 869–873; 10.1038/jp.2011.182 (2012).
14. Terwiel, J.Ph., Veltkamp, J.J., Bertina, R.M. & Muller, H.P. Coagulation factors in the human fetus of about 20 weeks of gestational age. *Br. J. Haematol.* **45**, 641–650; 10.1111/j.1365-2141.1980.tb07187.x (1980).
15. Terwiel, J.P., Veltkamp, J.J., Bertina, R.M., van der Linden, I.K. & van Tilburg, N.H. Coagulation factors in the premature infant born after about 32 weeks of gestation. *Neonatology* **47**, 9–18; 10.1159/000242085 (1985)
16. Andrew, M. *et al.* Development of the human coagulation system in the full-term infant. *Blood* **70**, 165–172 (1987).
17. Andrew, M. *et al.* Development of the human coagulation system in the healthy premature infant. *Blood* **72**, 1651–1657 (1988).
18. Reverdiau-Moalic, P., Delahousse, B., Body, G., Bardos, P. & Leroy, J. Evolution of blood coagulation activators and inhibitors in the healthy human fetus. *Blood* **88**, 900–906 (1996).
19. Heikinheimo, R. Coagulation studies with fetal blood. *Neonatology* **7**, 319–327; 10.1159/000239936 (1964).
20. Hsi, B.-L., Page Faulk, W., Yeh, C.-J.G. & McIntyre, J.A. Immunohistology of clotting factor V in human extraembryonic membranes. *Placenta* **8**, 529–535; 10.1016/0143-4004(87)90081-6 (1987).
21. Yang, T.L. *et al.* The structure and function of murine factor V and its inactivation by protein C. *Blood* **91**, 4593–4599 (1998).
22. Yang, T.L., Pipe, S.W., Yang, A. & Ginsburg, D. Biosynthetic origin and functional significance of murine platelet factor V. *Blood* **102**, 2851–2855; 10.1182/blood-2003-04-1224 (2003).
23. De Pablo-Moreno, J.A., Liras, A. & Revuelta, L. Standardization of coagulation factor V reference intervals, prothrombin time, and activated partial thromboplastin time in mice for use in factor V deficiency pathological models. *Front. Vet. Sci.* **9**, 846216; 10.3389/fvets.2022.846216 (2022).
24. Cui, J., O'Shea, K.S., Purkayastha, A., Saunders, T.L. & Ginsburg, D. Fatal haemorrhage and incomplete block to embryogenesis in mice lacking coagulation factor V. *Nature* **384**, 66–68; 10.1038/384066a0 (1996).
25. Weyand, A.C. *et al.* Analysis of factor V in zebrafish demonstrates minimal levels needed for early hemostasis. *Blood Adv.* **3**, 1670–1680; 10.1182/bloodadvances.2018029066 (2019).
26. Yang, T., Cui, J., Taylor, J., Yang, A., Gruber, S. & Ginsburg, D. Rescue of fatal neonatal hemorrhage in factor V deficient mice by low level transgene expression. *Thromb. Haemost.* **83**, 70–77; 10.1055/s-0037-1613760 (2000).
27. De Pablo-Moreno, J.A. *et al.* Development of a novel and viable knock-in factor V deficiency murine model: utility for an ultra-rare disease. *PLoS ONE* **20**, e0321864; 10.1371/journal.pone.0321864 (2025).
28. Connolly, A.J., Ishihara, H., Kahn, M.L., Farese, R.V. & Coughlin, S.R. Role of the thrombin receptor in development and evidence for a second receptor. *Nature* **381**, 516–519; 10.1038/381516a0 (1996).
29. Griffin, C.T. A role for thrombin receptor signaling in endothelial cells during embryonic development. *Science* **293**, 1666–1670; 10.1126/science.1061259 (2001).

30. Ong, K., Horsfall, W., Conway, E. & Schuh, A. Early embryonic expression of murine coagulation system components. *Thromb. Haemost.* **84**, 1023–1030; 10.1055/s-0037-1614166 (2000).
31. Xue, J. *et al.* Incomplete embryonic lethality and fatal neonatal hemorrhage caused by prothrombin deficiency in mice. *Proc. Natl Acad. Sci. USA* **95**, 7603–7607; 10.1073/pnas.95.13.7603 (1998).
32. Bermejo-Álvarez, P., Park, K.-E. & Telugu, B.P. Utero-tubal embryo transfer and vasectomy in the mouse model. *J. Vis. Exp.* **51214**; 10.3791/51214 (2014).
33. Lamas-Toranzo, I. *et al.* Strategies to reduce genetic mosaicism following CRISPR-mediated genome edition in bovine embryos. *Sci. Rep.* **9**, 14900; 10.1038/s41598-019-51366-8 (2019).
34. Joseph, B.C., *et al*. An engineered activated factor V for the prevention and treatment of acute traumatic coagulopathy and bleeding in mice. *Blood Adv*. **6**, 959–969; 10.1182/bloodadvances.2021005257 (2022).
35. Joseph, B.C., *et al*. Traumatic bleeding and mortality in mice are intensified by iron deficiency anemia and can be rescued with tranexamic acid. *Res. Pract. Thromb. Haemost.* **8**, 102543; 10.1016/j.rpth.2024.102543 (2024).
36. Cañete, A. *et al.* Characterization of a fetal liver cell population endowed with long-term multiorgan endothelial reconstitution potential. *Stem Cells* **35**, 507–521; 10.1002/stem.2494 (2017).
37. Sanchez, M. *et al.* An SCL 3′ enhancer targets developing endothelium together with embryonic and adult haematopoietic progenitors. *Development* **126**, 3891–3904; 10.1242/dev.126.17.3891 (1999).
38. Serrano, L.J. *et al.* Searching for a cell-based therapeutic tool for haemophilia A within the embryonic/foetal liver and the aorta-gonads-mesonephros region. *Thromb. Haemost.* **118**, 1370–1381; 10.1055/s-0038-1661351 (2018).
39. Birling, M.-C., Herault, Y. & Pavlovic, G. Modeling human disease in rodents by CRISPR/Cas9 genome editing. *Mamm. Genome* **28**, 291–301; 10.1007/s00335-017-9703-x (2017).
40. Serrano, L.J. *et al.* Development and characterization of a factor V-deficient CRISPR cell model for the correction of mutations. *Int. J. Mol. Sci.* **23**, 5802; 10.3390/ijms23105802 (2022).
41. Cardiero, G., Musollino, G., Prezioso, R. & Lacerra, G. mRNA analysis of frameshift mutations with stop codon in the last exon: the case of hemoglobins Campania [α1 cod95 (−C)] and Sciacca [α1 cod109 (−C)]. *Biomedicines* **9**, 1390; 10.3390/biomedicines9101390 (2021).
42. Iengar, P. An analysis of substitution, deletion and insertion mutations in cancer genes. *Nucleic Acids Res.* **40**, 6401–6413; 10.1093/nar/gks290 (2012).
43. Hart, D.P. FVIII immunogenicity—bioinformatic approaches to evaluate inhibitor risk in non-severe hemophilia A. *Front. Immunol.* **11**, 1498; 10.3389/fimmu.2020.01498 (2020).
44. Natalia, R., Jayne, L., Shawn, T., Paula, J. & David, L. The Canadian "National Program for hemophilia mutation testing" database: a ten-year review. *Am. J. Hematol.* **88**, 1030–1034; 10.1002/ajh.23557 (2013).
45. Peters, L.L. *et al.* Large-scale, high-throughput screening for coagulation and hematologic phenotypes in mice. *Physiol. Genomics* **11**, 185–193; 10.1152/physiolgenomics.00077.2002 (2002).
46. Delev, D., Pavlova, A., Heinz, S., Seifried, E. & Oldenburg, J. Factor 5 mutation profile in German patients with homozygous and heterozygous factor V deficiency. *Haemophilia* **15**, 1143–1153; 10.1111/j.1365-2516.2009.02048.x (2009).
47. Bernal, S. *et al.* High mutational heterogeneity, and new mutations in the human coagulation factor V gene. Future perspectives for factor V deficiency using recombinant and advanced therapies. *Int. J. Mol. Sci.* **22**, 9705; 10.3390/ijms22189705 (2021).
48. Schreuder, M., Reitsma, P.H. & Bos, M.H.A. Blood coagulation factor Va's key interactive residues and regions for prothrombinase assembly and prothrombin binding. *J. Thromb. Haemost.* **17**, 1229–1239; 10.1111/jth.14487 (2019).
49. Brooks, J.W. Postmortem changes in animal carcasses and estimation of the postmortem interval. *Vet. Pathol.* **53**, 929–940; 10.1177/0300985816629720 (2016).
50. Lippi, G. *et al.* Inherited and acquired factor V deficiency. *Blood Coagul. Fibrinolysis* **22**, 160–166; 10.1097/MBC.0b013e3283424883 (2011).
51. Hassan, H.J. *et al.* Blood coagulation factors in human embryonic-fetal development: preferential expression of the FVII/tissue factor pathway. *Blood* **76**, 1158–1164 (1990).
52. Kashif, M. & Isermann, B. Role of the coagulation system in development. *Thromb. Res.* **131**, S14–S17; 10.1016/S0049-3848(13)70012-4 (2013).
53. Naderi, M., Tabibian, S., Shamsizadeh, M. & Dorgalaleh, A. Miscarriage and recurrent miscarriage in patients with congenital factor V deficiency: a report of six cases in Iran. *Int. J. Hematol.* **103**, 673–675; 10.1007/s12185-016-1981-7 (2016).
54. Shibata, M., Makihara, N. & Iwasawa, A. The yolk sac's essential role in embryonic development. *Reprod. Med. Biol.* **11**, 243–258; 10.7831/ras.11.0_243 (2023).

55. Goh, I. *et al.* Yolk sac cell atlas reveals multiorgan functions during human early development. *Science* **381**, eadd7564; 10.1126/science.add7564 (2023).
56. Segers, K., Dahlbäck, B. & Nicolaes, G. Coagulation factor V and thrombophilia: background and mechanisms. *Thromb. Haemost.* **98**, 530–542; 10.1160/TH07-02-0150 (2007).
57. Liebman, H.A., Furie, B.C. & Furie, B. Hepatic vitamin K–dependent carboxylation of blood–clotting proteins. *Hepatology* **2**, 488S–494S; 10.1002/hep.1840020416 (1982).
58. Tatsumi, K. *et al.* Hepatocyte is a sole cell type responsible for the production of coagulation factor IX in vivo. *Cell Med.* **3**, 25–31; 10.3727/215517912X639496 (2012).
59. Jensen, A.H.-B., Josso, F., Zamet, P., Monset-Couchard, M. & Minkowski, A. Evolution of blood clotting factor levels in premature infants during the first 10 days of life: a study of 96 cases with comparison between clinical status and blood clotting factor levels. *Pediatr. Res.* **7**, 638–644; 10.1203/00006450-197307000-00007 (1973).
60. Huang, X. *et al.* Frame-shifted proteins of a given gene retain the same function. *Nucleic Acids Res.* **48**, 4396–4404; 10.1093/nar/gkaa169 (2020).
61. Shi, G.-D. *et al.* iTRAQ-based proteomics profiling of Schwann cells before and after peripheral nerve injury. *Iran. J. Basic Med. Sci.*; 10.22038/ijbms.2018.26944.6588 (2018).
62. Dai, Y., Kretz, C.A., Kim, P.Y. & Gross, P.L. A specific fluorescence resonance energy quenching–based biosensor for measuring thrombin activity in whole blood. *J. Thromb. Haemost.* **22**, 1627–1639; 10.1016/j.jtha.2024.02.007 (2024).
63. Krenzlin, H., Lorenz, V., Danckwardt, S., Kempski, O. & Alessandri, B. The importance of thrombin in cerebral injury and disease. *Int. J. Mol. Sci.* **17**, 84; 10.3390/ijms17010084 (2016).
64. Bhat, V. *et al.* Vascular remodeling underlies rebleeding in hemophilic arthropathy. *Am. J. Hematol.* **90**, 1027–1035; 10.1002/ajh.24133 (2015).
65. Wang, J., Zohar, R. & McCulloch, C.A. Multiple roles of α-smooth muscle actin in mechanotransduction. *Exp. Cell Res.* **312**, 205–214; 10.1016/j.yexcr.2005.11.004 (2006).
66. Ito, K. *et al.* An immunohistochemical analysis of tissue thrombin expression in the human atria. *PLoS ONE* **8**, e65817; 10.1371/journal.pone.0065817 (2013).

FIGURE LEGENDS

Fig. 1. Coagulometric measurements for WT and Hz groups. (A) FV activity expressed in UI/mL and percentage (n=6). (B) aPTT expressed in seconds (n=6). (C) PT expressed in seconds, percentage and INR (n=6). Calibration curves were generated using pooled wild-type (WT) plasma. The data are expressed as mean ± standard deviation. *$p<0.05$ according to Student's t test. Abbreviations: FV, factor V; Hz, heterozygous; INR, international normalized ratio; WT, wild type.

Fig. 2. Main pathological findings in newborn Hm individuals (A, B) and in the young Hm individual (C, F). (A, B) Extensive light red erythematous area with bright red multifocal hemorrhages, encompassing the skull, eyes, submandibular and cervical areas, anterior aspect of the thoracic region and proximal anterior limbs. (C, D) Sub meningeal multifocal hemorrhagic areas, mainly at the frontal and interparietal sutures (arrows). (E) Extensive hemorrhagic areas adjacent to the molecular layer of the hippocampal dentate gyrus (arrow) and multifocal hemorrhages occupying the molecular layer of the dentate gyrus (arrowhead). The cells comprising the molecular and polymorphic layers of the dentate gyrus present with cytoplasmic vacuolation. H&E stain, 10x. (F) Perivascular multifocal hemorrhages located in the neuropil of the thalamus (arrow); H&E stain, 10x. Abbreviations: Hm, homozygous.

Fig. 3. Distribution and location of thrombin in the brain cells of newborn Hm mice (A) and the young Hm individual (C), as seen by immunohistochemistry analysis. Images from newborn WT animals (no mutation) (B) and adult WT animals (no mutation) (D). (A) Minimal immunolabeling in the neurons' cytoplasmic projections (arrow) close to the

subarachnoid space, which was full of erythrocytes; rabbit polyclonal anti-thrombin antibody, 40x. (B) Moderate immunolabeling in the neurons' cytoplasmic projections (arrow) close to the subarachnoid space; rabbit polyclonal anti-thrombin antibody, 40x. (C) No immunolabeling was observed in the neurons' cytoplasm within the thalamus, adjacent to perivascular hemorrhagic areas (arrowhead); rabbit polyclonal anti-thrombin antibody, 20x. Inset: Minimal immunolabeling in the cytoplasm of the neurons close to the ependyma, 40x. (D) Intense immunolabeling in the dendritic projections of the neuronal cytoplasm and glial cells within the thalamus (arrow); rabbit polyclonal anti-thrombin antibody, 20x. Abbreviations: Hm, homozygous; WT, wild type.

Fig. 4. Distribution and location of factor V in liver (A, B) and brain cells (C, D) of newborn Hm individuals (A) and of the young Hm individual (C) as seen by immunohistochemistry analysis. Images from newborn WT animals (B) and adult WT animals are included (D). (A, B) Moderate immunolabeling in the cytoplasm of hepatocytes and the Kupffer cells (arrow); rabbit polyclonal anti-FV antibody, 40x. (C) No immunolabeling in the neurons' cytoplasm; rabbit polyclonal anti-FV antibody, 40x. (D) Moderate immunolabeling in the neuronal cytoplasm (arrow); rabbit polyclonal anti-thrombin antibody, 40x. Abbreviations: Hm, homozygous; WT, wild type.

Fig. 5. Immunolabeling of blood vessels in the presence of α-SMA in the liver (A, B) and the heart (C, D) of newborn Hm individuals (A, C), as seen by immunohistochemistry analysis. Images from newborn WT animals are included (B, D). (A) Slight immunolabeling in centrilobular veins and in the vessels of the portal space (arrow); mouse anti-α-SMA monoclonal antibody, 4x. Inset: slight immunostaining of the cells of the centrilobular vein wall, 40x. (B) Intense immunolabeling in the centrilobular veins and in the vessels of the portal space (arrow); mouse anti-α-SMA monoclonal antibody, 4x. Inset: intense immunostaining of the cells of the centrilobular vein walls, showing a thickened vascular wall, 40x. (C) Slight immunolabeling in the myocardial vessels; anti-α-SMA monoclonal antibody in the mouse, 20x. (D) Intense immunolabeling in myocardial vessels and moderate immunolabeling in cardiomyocytes; mouse anti-α-SMA monoclonal antibody, 20x. Abbreviations: Hm, homozygous; WT, wild type.

Fig. 6. Immunolabeling of blood vessels in the presence of α-SMA in the liver (A, B) and the heart (C, D) of the young Hm individual (A, C) as seen by immunohistochemistry analysis. Images from WT animals (no mutation) (B, D). (A) Interrupted immunolabeling in the portal vein and attenuated response in the hepatic artery (arrow); mouse anti-α-SMA monoclonal antibody, 40x. (B) Homogeneous immunolabeling in the portal vein and intense immunolabeling in the hepatic artery (arrow); anti-α-SMA monoclonal antibody in the mouse, 40x. (C) Interrupted immunolabeling in the myocardial vessels (arrow); mouse anti-α-SMA monoclonal antibody, 20x. (D) Homogeneous immunolabeling in the myocardial vessels; mouse anti-α-SMA monoclonal antibody, 20x. Abbreviations: Hm, homozygous; WT, wild type.

Fig. 7. Relative expression of the *F5* gene (n=3-4) at various stages of embryonic development and in adult mouse liver (mean ± standard deviation). Significant differences are indicated by lines and asterisks (*$p<0.05$) according to Welch's ANOVA. Abbreviation: E, embryonic stage.

Fig. 8. Relative expression of the *F5* gene ($2^{-\Delta Ct}$) across different tissues at stages E9.5, E10, E11 and E12. On the left of the graph, values are represented as mean ± standard

deviation (SD), whereas on the right, they are shown as median and range. Significant differences are indicated by lines and asterisks (*p<0.05) according to Welch's ANOVA or Krustal Wallis. Abbreviations: AGM, aorta-gonad-mesonephros region.

Fig. 9. Relative expression of the *F5* gene ($2^{-\Delta Ct}$) across different tissues at the various stages. (A) Stage E9.5 (median and range). (B) Stage E10 (median and range). (C) Stage E11 (mean ± SD). (D) Stage E12 (median and range). Significant differences are indicated by lines and asterisks (*p<0.05) according to Welch's ANOVA or Krustal Wallis. Abbreviations: AGM, aorta-gonad-mesonephros region.

TABLE LEGENDS

Table 1. Genotyping primers. [a]llumina MiSeq System sequencing overhangs are identified in italics within the genotyping primers; WT bp: size of the wild-type product expressed in base pairs.

Table 2. Antibodies for immunohistochemical study. All antibodies were purchased from Thermo Fisher Scientific.

Table 3. qPCR primers.